ARTICLE

Supporting Information for

Pure Metallic Nanofibrillar Membrane for High Performance Electrostatic Air Filtration with Antimicrobial and Reusable Characteristics

Seunghun Yoo, Inyeong Yang, Ji-hun Jeong, Jihae Chang, Sanha Kim*

Department of Mechanical Engineering, Korea Advanced Institute of Science and Technology (KAIST), 291 Daehak-ro, Yuseong-gu, Daejoeon 34141, Republic of Korea

*email: sanhkim@kaist.ac.kr

Scalable fabrication of the nanofibrillar copper network

The main components of the electrodeposition system used for the growth of Cu nano dendrites are a Cu woven mesh (working electrode), a Cu plate (counter electrode), an electrolyte and a power supply, Fig. S1a. The Cu woven mesh was a commercial product in which 30 μm diameter wires are crossed, Fig. S1b, and when electrodeposition is performed, nano sized Cu dendrites fill the open areas of the Cu woven mesh, Fig. S1c

The process variables that can control the shape and arrangement of Cu nano dendrites in the electrodeposition process are the concentration and additives of the electrolyte, the voltage applied to the two electrodes, and the deposition time. In this work, the shape and arrangement of Cu nano dendrites suitable for filter application were achieved by controlling the voltage and time applied during the electrodeposition. If the applied voltage is increased, the current concentration is strengthened, so that the diameter of the Cu nano dendrites is reduced (1.78 μm at 4.8V), and the arrangement becomes non-uniform. Conversely, if the applied voltage is lowered, the diameter of the Cu nano dendrites increases (3.11 μm at 1.2 V), and the arrangement becomes uniform.

In order to have high filter efficiency, the diameter of the Cu nano dendrites must be small, so in this work, electrodeposition was performed at a maximum voltage of 2.4 V within the range for uniform electrodeposition, Fig. S2a. As the electrodeposition time increased, the amount of Cu nano branches increased, and the thickness of the filter increased (445 μm at 120s and 585 μm at 900s). For a high-performance filter, the filter efficiency should be high while the pressure drop should be low. Therefore, in this work, the electrodeposition was carried out with a minimum time of 300 s, which is a sufficient time to evenly fill the pores of the Cu woven mesh, Fig. S2b.

Cu nano dendrites formed by electrodeposition are made by anisotropic growth, so their uniformity is poor from a nano- and micro-microscopic point of view. To improve this, roll compression was performed.

As the compression pressure increases, the Cu nano dendrites are uniformly arranged, and the thickness of the filter is reduced, Fig. S3a. There was no change in the thickness of the filter at a pressure of 75 kgf or more and tearing of the filter occurred at a pressure of 150 kgf or more, Fig. S3b. In this work, roll compression was performed at a pressure of 100 kgf to maximize uniformity and minimize thickness without tearing.

The compressed Cu nano filter was vacuum heat treated immediately, as sintering. Heat was supplied by a coil wrapped around the glass quartz tube. The inside of the glass quartz tube was maintained in a vacuum state using an air compressor, and Ar gas was flowed at 1 L/min to prevent oxidation or chemical reaction of the Cu. The filter was placed on a graphite plate to enhance heat transfer, Fig. S4a. In the Cu filter before heat treatment, each Cu nano branch was arranged independently, Fig. S4b, whereas in the Cu filter after heat treatment, the Cu nano branches are connected through sintering, Fig. S4c. This not only prevents the Cu nano branches from falling off, but also improves the electrical particle collecting ability of the filter, by improving electrical conductivity.

The series of processes for fabricating Cu nano filters can be easily scaled up. Fig. S5a and b shows the change in the process system for scale-up and the result of scale-up of the Cu nano filter in this work. Cu nano branches were grown under the same voltage condition by increasing the size of the electrolyte tank of the electrodeposition system and the jig for fixing each electrode to manufacture a 120 mm square Cu nano filter, which is 2.4 times bigger than the size of the initial 50 mm square Cu nano filter. After that, roll compression and vacuum heat treatment were performed under the same conditions used for manufacturing the existing Cu nano filter. An optical picture, Fig. S5c, and an SEM image, Fig. S5d, confirm that the Cu nano branches were uniformly grown over the entire area even when the scale-up progresses.

Characterization of the nanofibrillar copper network

The components of the fabricated Cu nano filter was investigated using x-ray photoelectron spectroscopy (XPS) and energy dispersive x-ray spectroscopy (EDX). The XPS results of the Cu woven mesh before electrodeposition and the fabricated Cu nano filter were compared, Fig. S6a. The peaks of the two samples appeared the same over the entire range (0-1200 eV), and the same was also observed when the range of the Cu component (930-955 eV). Also, the signal for O was not seen in the EDX image of the Cu nano filter, Fig. S6b, and there was almost no difference in the atomic % of Cu in the EDX component table for the Cu woven mesh (95.75%) and the Cu nano filter (95.65%). The results confirmed that the Cu nano filter is made of pure Cu without any chemical transformation such as oxidation that may have occurred during the manufacturing process steps of electrodeposition, roll compression, and heat treatment.

The particle collection principle of the filter is divided between physical filtering and electrical filtering, Fig. S7. Physical filtering includes diffusion, sieving, interception, and inertial impaction. Which one is dominant depends on diverse conditions, such as particle size, flow rate, and fiber diameter. However, there is a limit: strengthening the physical filtering tends to increase the pressure drop of the filter. Therefore, this work was conducted to focus on the electrical filtering and improve it.

Electrical filtering includes collection by Coulomb force when particles and filter fibers are oppositely charged, and collection by induced polarization when only one of them is charged. Since the capture by Coulomb force is much stronger than that by induced polarization, in this work, the particles were charged negatively and the filter was positively charged, to employ collection by Coulomb force.

Theoretical analysis of the nanofibrillar Cu filter performance

To verify the suitability of the modelling equation, the pressure drop according to the flow rate of various Cu nano filter samples were measured and calculated for comparison, Fig. S8. It can be seen that the modelled differential pressure and the measured differential pressure are in good agreement with each other in the graph, and $R^2 = 0.9984$ with the $x = y$ graph.

The filter characteristic variables that can change the pressure drop in the modeling equation are porosity, diameter, and thickness. The change in the pressure drop of the filter for each condition was calculated by modeling, Fig. S9. As the porosity increased, the pressure drop of the filter decreased, and as the diameter increased, the pressure drop of the filter decreased. As the thickness increased, the pressure drop of the filter increased, but this change was not large compared to the variables of porosity and diameter. Therefore, in this work, we found and applied a process that can increase the porosity and branch diameter of the Cu nano filter.

Cleaning solvent for validation of reusability

We measured the dust holding capacity of our filter in an extremely polluted environments to first contaminate the filter to a lever that affects the filter performance. The filtration was continued until the pressure drop of the filter increases by 25%, then the weight of the filter was compared with the as-fabricated filter. The increased mass was calculated by subtracting the mass of the filter before and after polluted. The mass of holding dust was only 3% of a new filter, as the high density of the copper material. Accordingly, our metal nanofibrillar filters may withhold sufficient amount of dust before it reaches the contaminant level for cleaning. The contaminated filter was washed with various solvents and the changes in the Cu nano filter were observed with SEM to find a suitable solvent for cleaning, Fig. S10. The fabricated Cu nano filter was polluted by filtering incense smoke, until incense smoke particles blocked the pores of the filter. When it was washed in deionized water for 3 minutes, the incense smoke particles still remained. After washing in HCl for 3 minutes, some of the incense smoke particles were removed and the overall shape was restored, but particles still remained between the fine branches. If washing was performed in acetone for 3 minutes, even the incense smoke particles between the fine branches were removed and the filter returned to the uncontaminated filter state. This is because incense smoke particles are mainly composed of a carbon component, and acetone is a representative solvent of the carbon component, so the

particles were dissolved without damage to the branches. In general, about 70% of fine dust is also carbon, so acetone can be used as an effective cleaning agent in real situations.

Repeated experiments were conducted to confirm that acetone washing does not affect the performance of the filter by reusing. Filter efficiency and pressure drop were measured during the 20 cycles of repeated cleaning and filtration, Fig S11. After 20 cycles of reuse, the pressure drop increased 10 % while filter efficiency remained the same. The surface characteristics of the Cu nano filter before and after used were taken by SEM and EDX images, Fig. S12. The SEM images show no change in the shape of copper nanonetwork and diameter of nano Cu branches. EDX images show surface chemical composition before and after used. The chemical composition also remains unchanged within a margin of error after reusing. Thus, the copper nano filter in this study can be reused over dozens of times after proper cleaning which significantly increases the lifespan of the filter.

ZnO coated copper nano filter

To prevent the oxidation of copper we coated ZnO via ALD. ALD offers a few nanometer coating, and thereby enables no effect on the electrostatic particle capture mechanism. ZnO was accepted since the ZnO has both antioxidize and antibacterial properties. The filter performances before and after ZnO coating were measured as Fig S13. At 20 V applied to the filter as-fabricated filter showed 99.7% filter efficiency whereas the ZnO coated filter showed 99.6% filter efficiency. In addition, there was almost no change in pressure drop (62 Pa to 65.8 Pa). Furthermore, ZnO-coated filter showed antibacterial performance of 99.7% after 1 hour and 99.9% after 24 hours, under condition of using *S. aureus* bacterial suspension at a concentration of 2.6×10^4 cfu/ml.

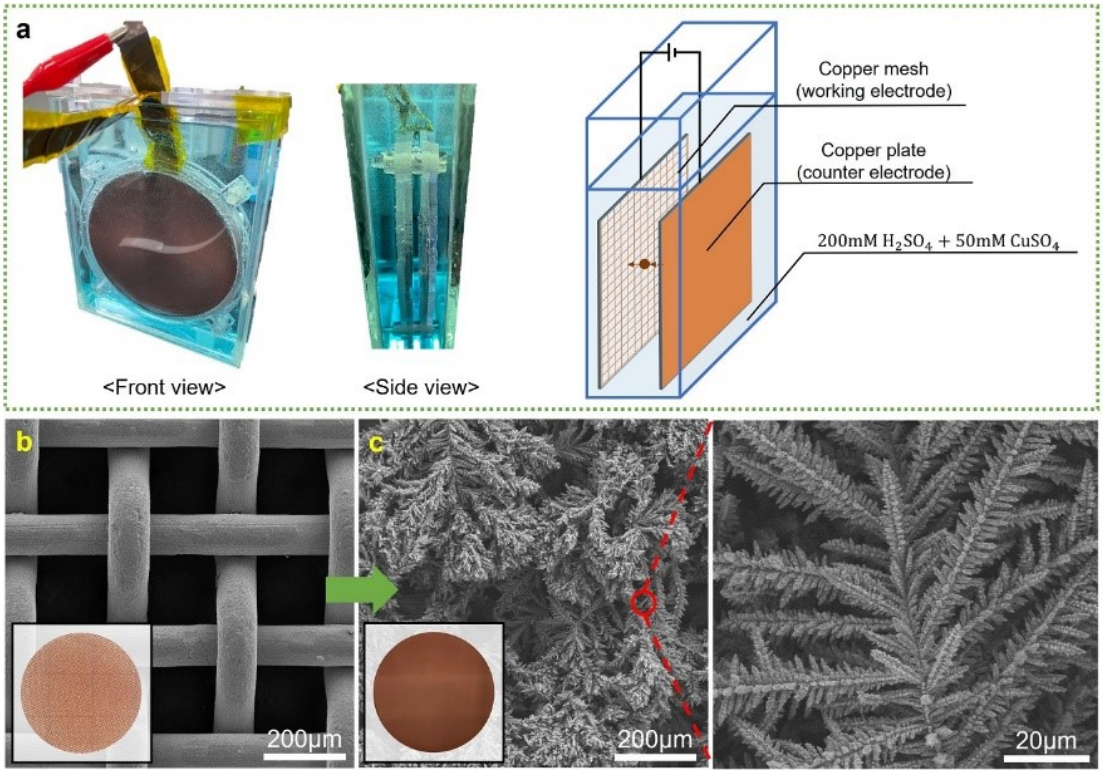

Fig. S1. Electrodeposition system. (a) Optical images and a schematic diagram of the electrodeposition apparatus, (b) an optical and a SEM image before electrodeposition, and (c) an optical and SEM images after electrodeposition.

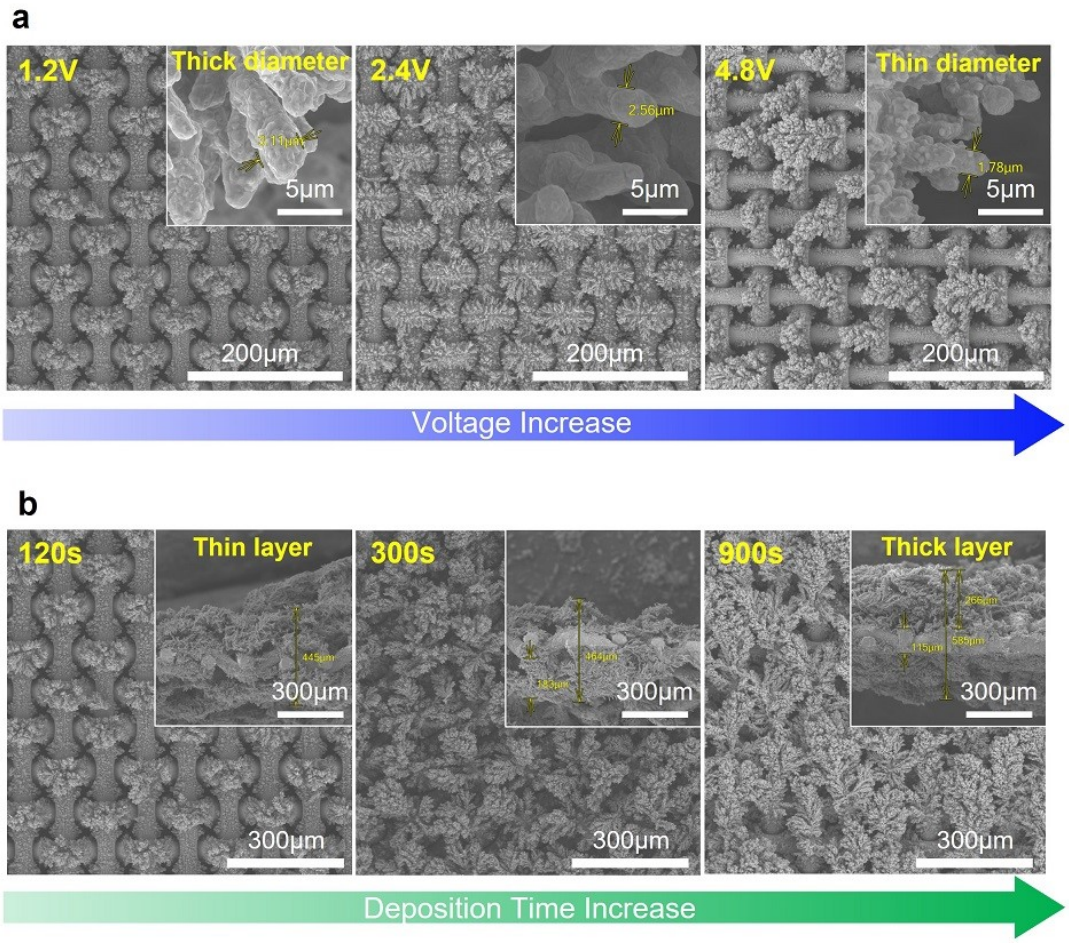

Fig. S2. Electrodeposition variables for controlling the growth of the Cu nano branches. SEM image of shape change under various electrodeposition conditions according to (a) voltage during electrodeposition, (b) electrodeposition time.

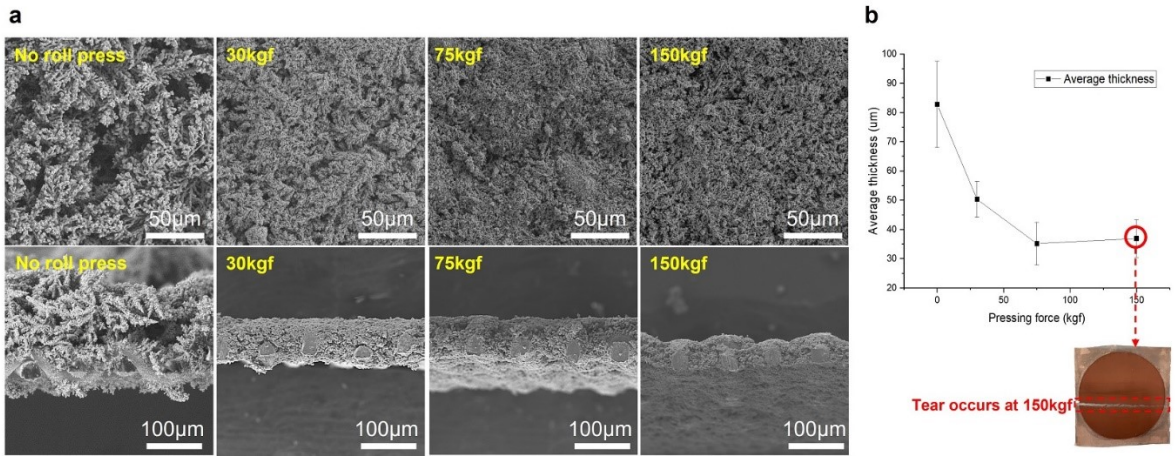

Fig. S3. Roll compression of the nanofibrillar Cu network. (a) SEM images showing the arrangement of Cu nano fibers and the thickness of the filter according to the pressure, and (b) measured thickness of nanofibrillar Cu network according to the roll compress pressure.

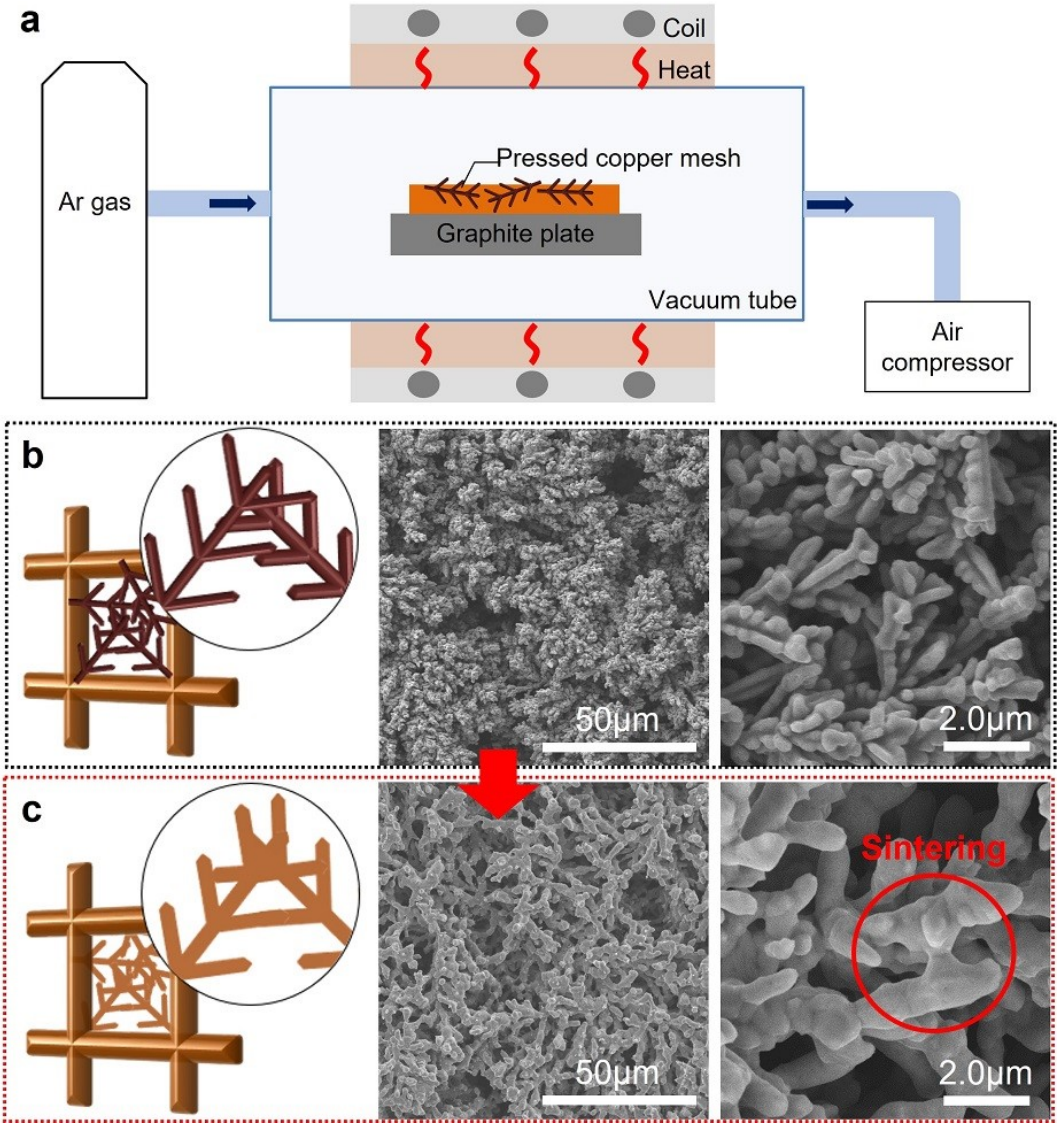

Fig. S4. Thermal sintering of the nanofibrillar Cu network. (a) Schematics of vacuum heat treatment system used for the thermal sintering, (b) an illustration and SEM images showing the Cu nano fibers before thermal sintering, and (c) an illustration and SEM images showing the Cu nano fibers after thermal sintering.

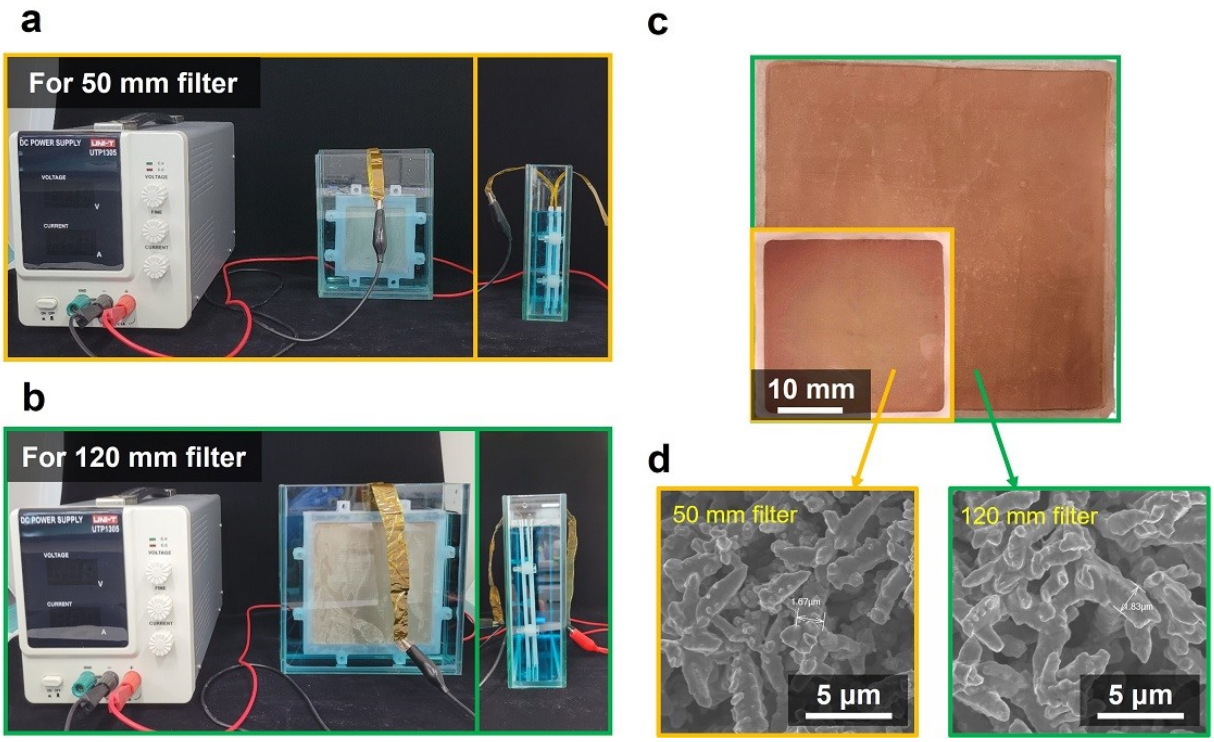

Fig. S5. Scaled-up fabrication of the nanofibrillar Cu network. (a) A photograph of electrodeposition system used for fabricating the 50 mm sized nanofibrillar Cu network, and (b) a photograph of electrodeposition system used for fabricating the 120 mm sized nanofibrillar Cu network. (c) A photograph of the nanofibrillar Cu network with and without scale up, and (d) SEM images showing the magnified image of each nanofibrillar Cu network.

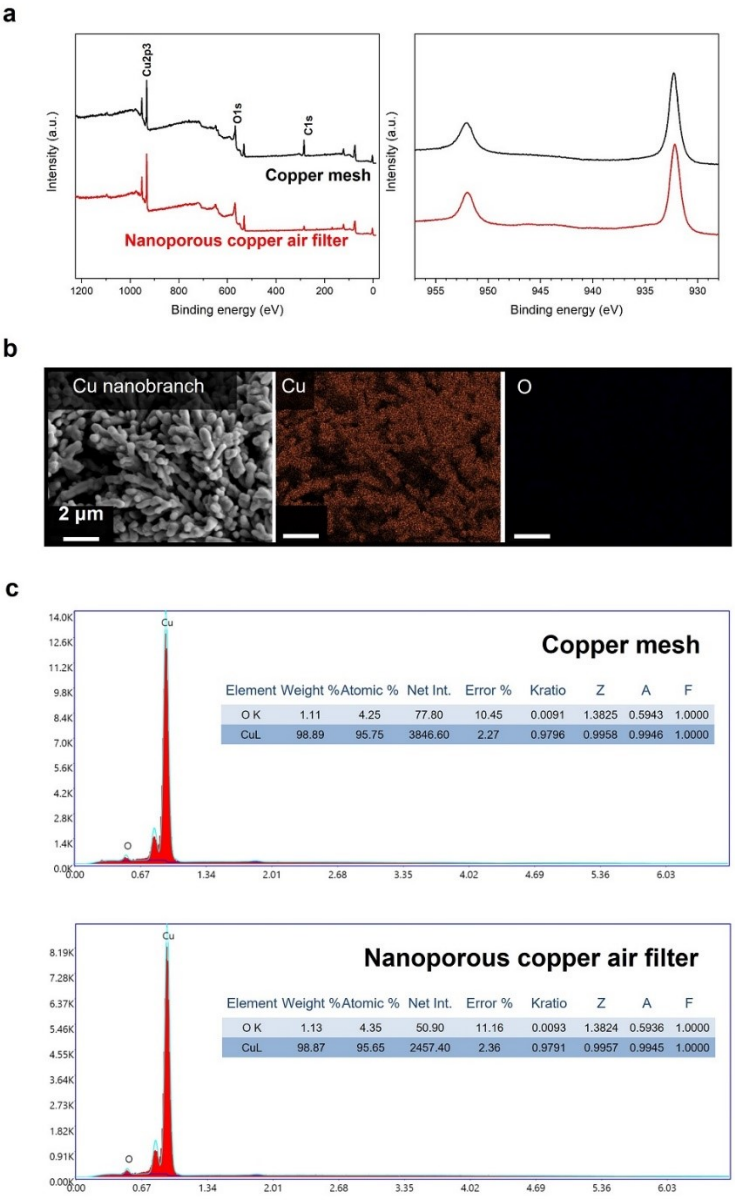

Fig. S6. Characteristics of the nanofibrillar Cu network. (a) XPS results of the woven Cu mesh and nanofibrillar Cu network, (b) EDS image results of the nanofibrillar Cu network, and (c) EDX composition results of the woven Cu mesh and nanofibrillar Cu network.

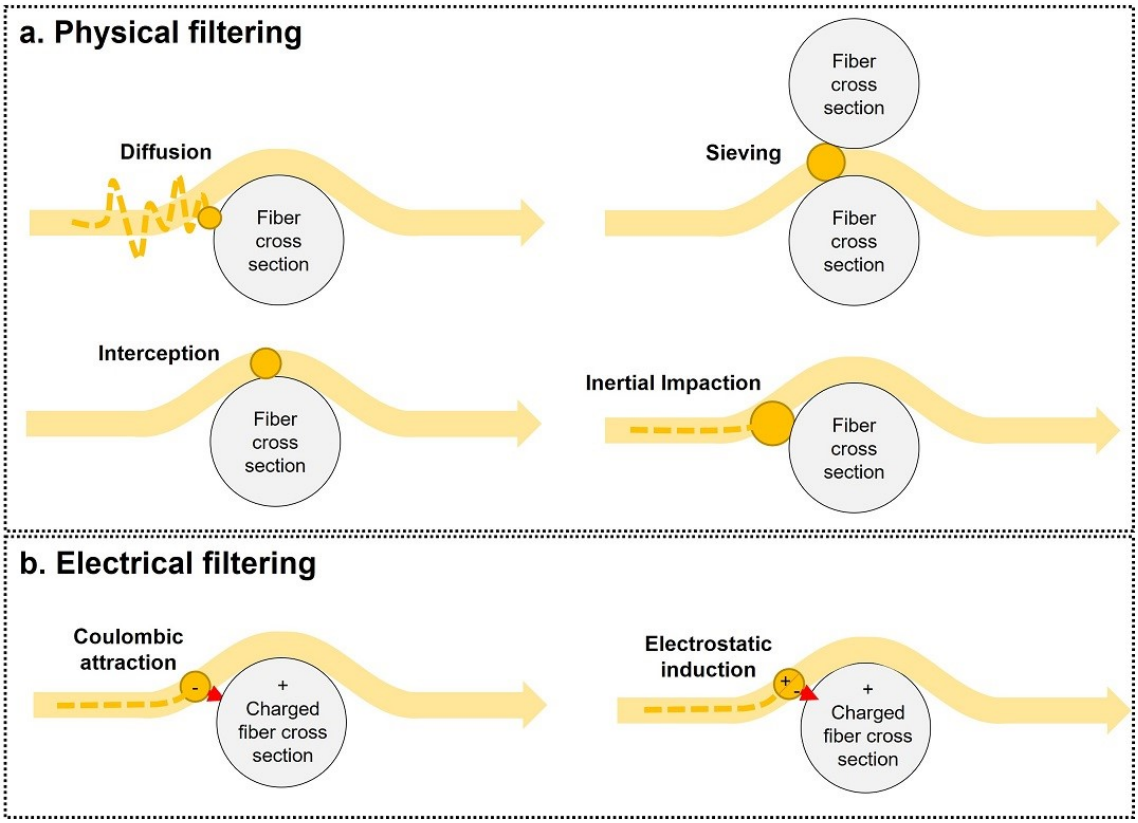

Fig. S7. Filtration mechanisms of the air filter. Schematic diagram of filtration mechanism of the air filter showing the (a) Physical filtration mechanism, and (b) electrostatic filtration mechanism.

Table S1. Ozone concentration in the Cu nano filter system.

Ionizer	Ozone concentration	Increment
Off	0.03 ppm	-
On	0.03 ppm	<0.01 ppm

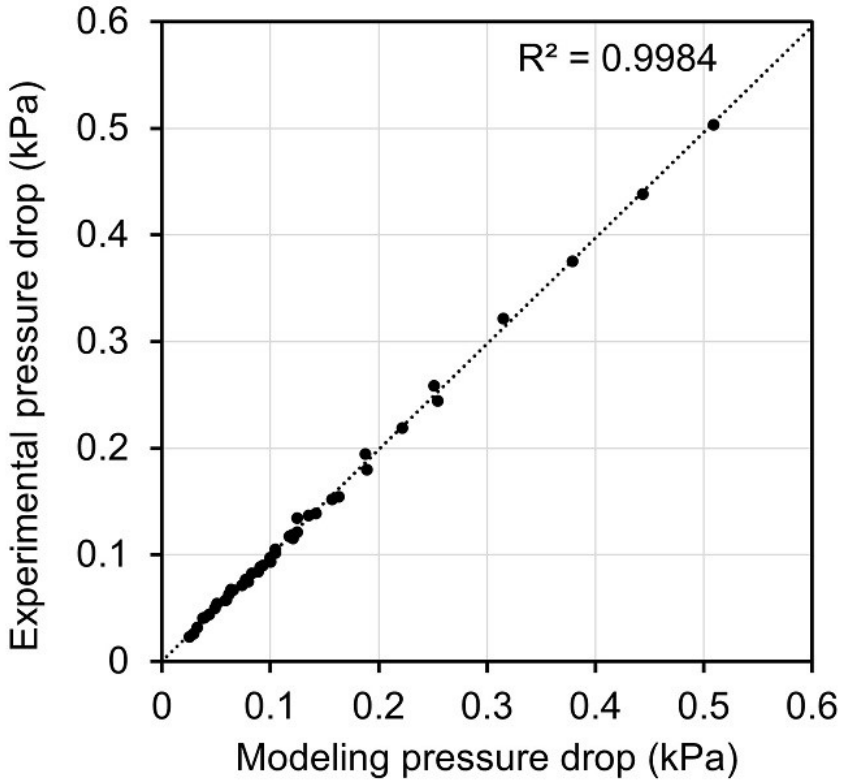

Fig. S8. Reliability of modelling of the nanofibrillar Cu network. Pressure drop of the nanofibrillar Cu networks were measured and calculated for various conditions and the results plotted.

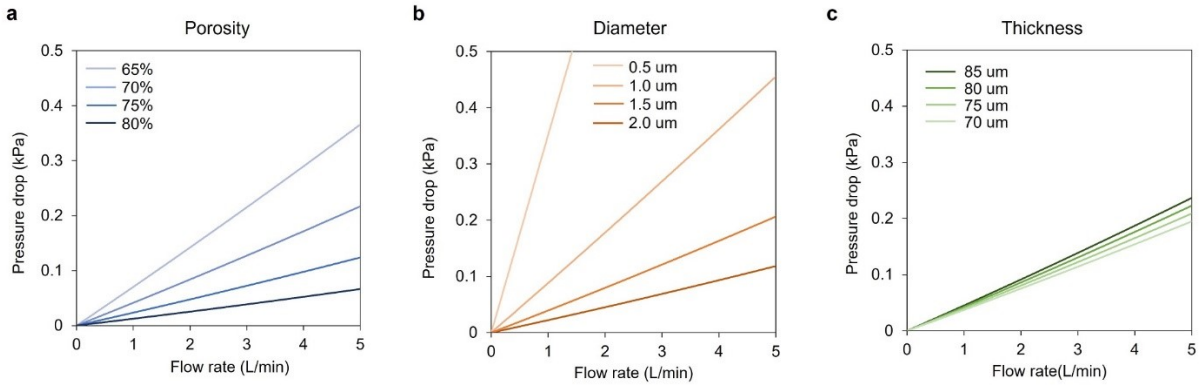

Fig. S9. Change in pressure drop according to the characteristics of the nanofibrillar Cu network.

Pressure drop calculated via modeling according to the (a) porosity, (b) branch diameter, and (c) thickness.

Table S2. Relative weight of the holding dust in copper nano filter.

As- fabricated filter	After pressure drop increases 25%	Holding dust	Relative weight
1.1398 g	1.1744 g	0.0346 g	3.04%

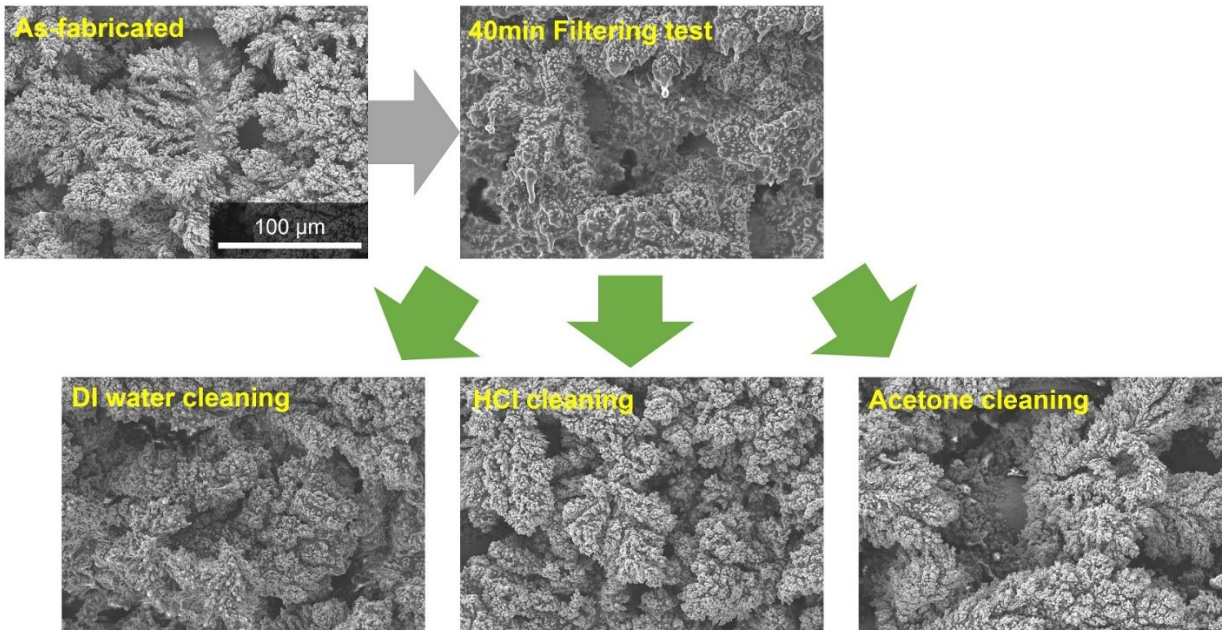

Fig. S10. Cleaning performance according to the solvents. SEM images of nanofibrillar Cu network as fabricated, after 40 min incense particle contamination, Deionized water washing, acetone washing, and HCl washing.

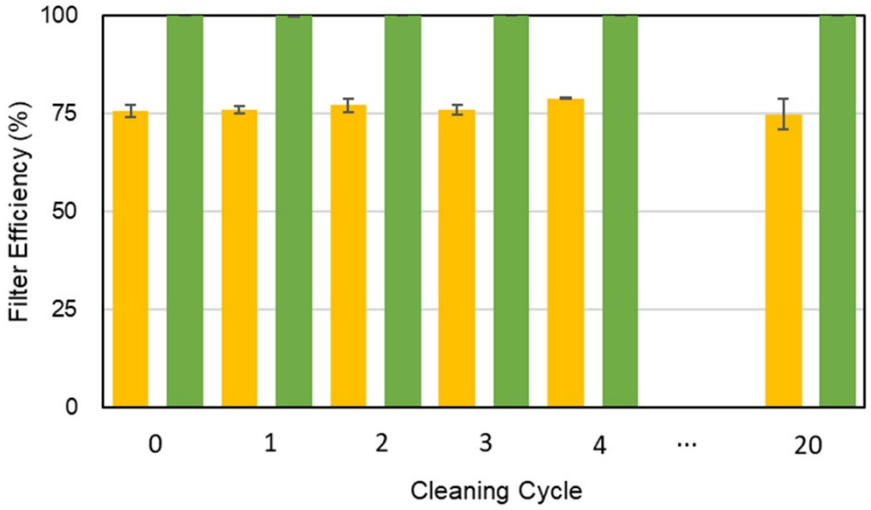

Cycle	0	1	2	3	4		20
Pressure Drop	62 Pa	70 Pa	69.8 Pa	70.6 Pa	70.6 Pa		69.4 Pa

Figure S11. Filter efficiency and pressure drop of the copper nano filter over cleaning iteration. 10 min of filtration test and 10 min of washing in acetone were repeated. The filter efficiency and the pressure drop were measured after each cycle.

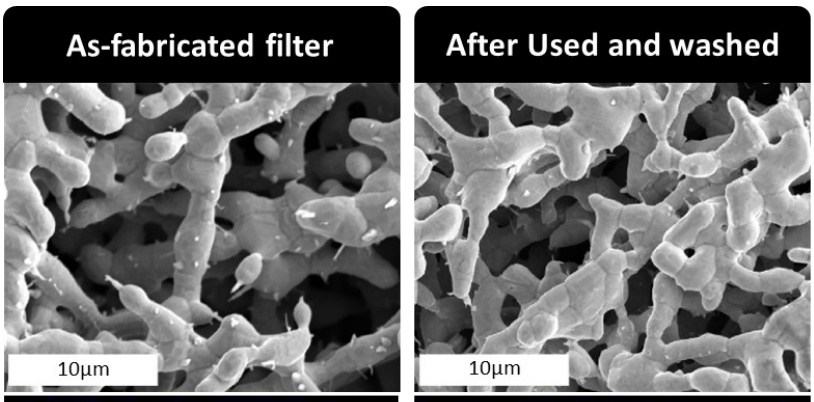

Element	Weight %	Error %	Element	Weight %	Error %
O K	1.8	8.5	O K	2.3	9.2
Cu L	98.2	5.4	Cu L	97.7	5.5

Figure S12. Surface characteristics of the Cu nano filter before and after filtration and cleaning.

In EDX images, blue dots indicate the oxide atom and the red dots indicate the copper atom on the surface.

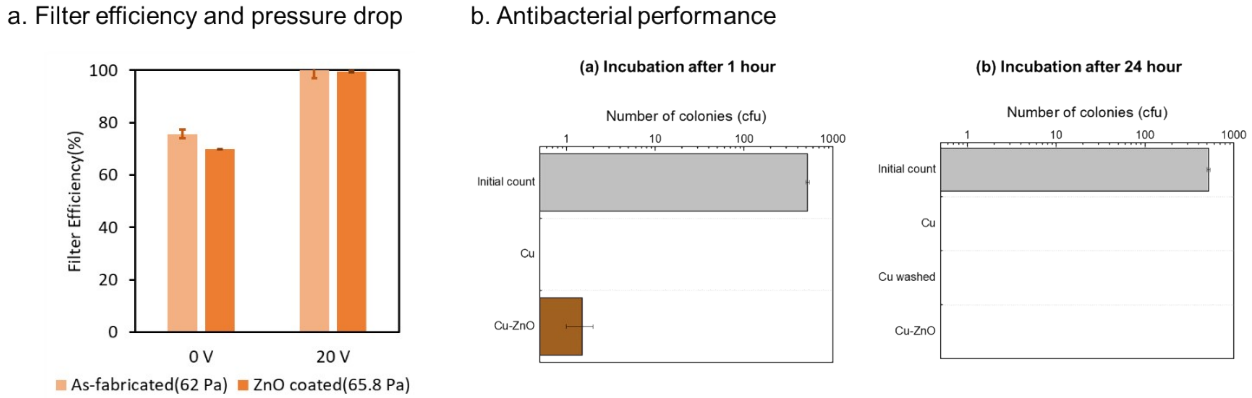

Figure S13. Comparison of the filter performance before and after ZnO coating via ALD. (a) Filter efficiency at 0V and 20V of as-fabricated and of ZnO coated filters are plotted. The pressure drop of each filter are listed below the plot. (b) Antibacterial performances of filter before and after the ZnO coating after 1 hour of incubation (left) and 24 hours of incubation (right).